# Histogram-Based Flash Channel Estimation

Haobo Wang, Tsung-Yi Chen, and Richard D. Wesel
whb12@ucla.edu, tsungyi.chen@northwestern.edu, wesel@ee.ucla.edu

***Abstract*—Current generation Flash devices experience significant read-channel degradation from damage to the oxide layer during program and erase operations. Information about the read-channel degradation drives advanced signal processing methods in Flash to mitigate its effect. In this context, channel estimation must be ongoing since channel degradation evolves over time and is a function of the number of program/erase (P/E) cycles. This paper proposes a framework for on-line model-based channel estimation using limited channel measurements (reads). This paper uses a channel model characterizing degradation as a function of retention time and the amount of charge programmed and erased. For channel histogram measurements, equal-probability (equal-height) bin placement yields a good approximation to the original distribution using only ten bins (i.e. nine reads). With the channel model and binning strategy in place, this paper explores candidate numerical least squares channel estimation algorithms and ultimately demonstrates the effectiveness of the Levenberg-Marquardt algorithm, which provides both speed and accuracy, in an algorithm for voltage allocation.**

***Index Terms*—Flash, Channel Estimation, Least Square, Binning Strategy**

## I. INTRODUCTION

With widespread use in computers, phones and even satellites, Flash memory has become one of the key components directly contributing to the fast-paced evolution of electronic systems. However, the reliability of Flash memory degrades with respect to usage and retention time. Both the extent of usage and the maximum allowed retention time before which data can be reliably recovered are limited. This causes significant drawbacks in practical applications. Furthermore, physical cell density and modulation constellation density (number of levels) are increasing rapidly to satisfy the demand for increased storage capacity under strict physical size constraints. This amplifies the degradation problem.

Modern Flash storage solutions employ channel codes [1], [2] to increase reliability, but this approach alone cannot effectively counteract the channel capacity decrease caused by degradation from recursively programming and erasing the cells. Signal processing methods such as Dynamic Voltage Allocation (DVA) [3] and Dynamic Threshold Assignment (DTA) [4] actively mitigate channel degradation. Effective decoding of channel codes, variable selection of channel code rates, and adaptive signal processing such as DVA and DTA require channel state information. Thus, it is necessary to have a robust on-line estimation framework for this evolving channel.

This work was supported by a grant from Western Digital Corporation and by the Center on Development of Emerging Storage Systems (CoDESS) http://www.uclacodess.org.

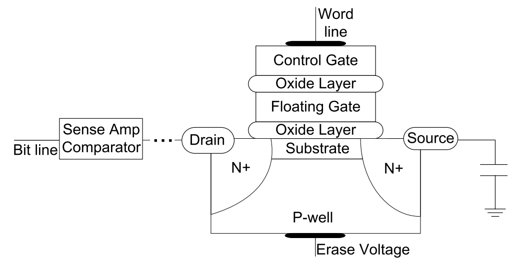


Fig. 1. Common structure of a P-well Flash memory cell.

Fig. 1 shows basic physical structure for a P-well Flash memory cell. The threshold voltage of a Flash cell is largely determined by the amount of charge in the floating gate and the device's intrinsic (charge-neutral) threshold voltage. Electrons are programmed to and erased from the floating gate through the oxide layer. As a result, the threshold voltage can be controlled by program and erase (P/E) operations [5]. Information about the threshold voltage can be obtained by applying a word line voltage and reading the sense amplifier output to determine if the threshold voltage has been surpassed. Due to channel degradation, the measured value of the threshold voltage often differs from the originally stored threshold voltage.

This paper explores histogram-based channel estimation (HBCE) for Flash. For a given block, multiple sense amplifier reads at distinct wordline voltages yield a histogram of the operational threshold voltages. This histogram provides an estimate for the actual read channel distribution.

In [6], the authors demonstrate that a multimodal Gaussian distribution representing four-level MLC Flash can be accurately estimated by least squares (LS) with 12-bin histograms using the Levenberg-Marquardt (LM) algorithm. In [6] eight parameters are estimated, four means and four variances.

Our work is largely inspired by [6]. We apply HBCE to a read-channel distribution that models the device physics for degradation, namely wear-out and retention loss. By modeling the underlying physical properties, our channel model uses fewer parameters (five) to characterize the channel. The combination of fewer parameters and the use of an improved binning paradigm allows LM to accurately estimate a more detailed channel distribution using only 10-bins.

The remainder of this paper is organized as follows: Section II presents the Flash channel model used in the paper. Section III compares three binning strategies from the perspectives of squared Euclidean distance and effective resolution. Section IV compares three least squares channel parameter estimation algorithms in terms of their speed and accuracy in estimating channel parameters that minimize the squared Euclidean distance between the measured histogram and the histogram produced by the estimated channel parameters in the context of our channel model. Section V presents simulation results demonstrating that a 10-bin (9-read) histogram with an equal-probability binning strategy and Levenberg-Marquardt least squares algorithm provides excellent channel parameter estimations and provides good performance in a DVA algorithm. Section VI concludes the paper.

## II. Flash Memory Channel Model

Recent research in Flash provides many good channel models. We utilize the model presented in [3] for our analysis. This model provides a tractable and realistic approach for approximating asymmetric Flash read-channel noise.

### A. Degradation Mechanism

Based on the literature [7]–[9], two important forms of degradation are investigated in our analysis. The first one is called wear-out, which is the P/E cycling-related degradation. The second mechanism, which is called retention loss, is also caused by the P/E cycling. The key distinction between wear-out and retention loss is that variations in threshold due to wear-out can be measured immediately after writing and variations in threshold due to retention loss occur over the period of retention time. Retention loss becomes more severe with longer retention time.

Because Flash cells are densely packed in a two dimensional array in the chip, the coupling effect among the cells causes the distortion of the channel known as cell-to-cell interference. This interference depends on the specific structure of individual Flash chip and the operation sequence of the controller [10], [11]. As a result, channel models including cell-to-cell interference are highly implementation dependent. Thus, in this paper, cell-to-cell interference is not modeled. Many methods counteracting this problem have been proposed in the semiconductor community, such as P/E sequence optimization and write voltage pre-distortion [11], [12].

Similarly, read disturb is implementation dependent and not included in our model. However, given the implementation details, we believe that both read disturb and cell-to-cell interference *could* be incorporated in a general channel model used for histogram-based estimation.

### B. Channel Model

Based on the theoretical analysis and experimental results from the literature [7]–[9], [12]–[14], our Flash memory channel model is formulated with three additive noise components:

$$y = x + n_p + n_w + n_r\,, \tag{1}$$

where $x$ is the intended threshold voltage written to a cell, and $y$ is the measured threshold voltage. The component $n_p$ is the programing noise related only to the programming process, $n_w$ denotes the wear-out noise, and $n_r$ represents the retention noise caused by retention loss.

Fig. 2 shows an example channel distribution, which demonstrates the impact of the noise components to the channel.

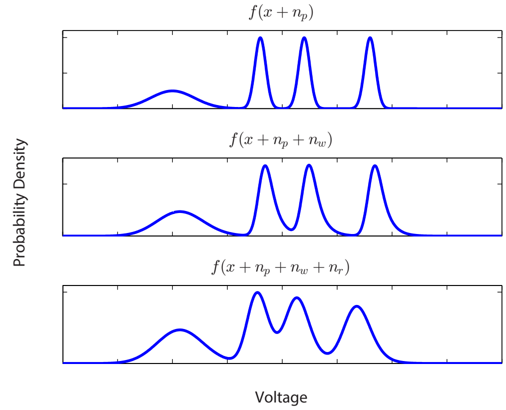


Fig. 2. Flash read channel probability density functions (PDFs) illustrating degradation mechanisms.

*1) Programming Noise:* The uncertainty of programmed or erased threshold voltages measured immediately after the programming or erase operation of a new Flash memory cell (that has no wear-out) can be modeled by Gaussian distribution. The variance of the distribution depends on cell's stored state, [12]–[14]. Let $l$ denotes the level of intended threshold with $l = 0$ representing the erased state and $l > 0$ representing programmed states. Programming Noise can then be modeled as

$$f_{N_P}(n_p|l) = \begin{cases} \mathcal{N}(0, \sigma_p^2) & \text{if } l = 0, \\ \mathcal{N}(0, \sigma_e^2) & \text{if } l > 0. \end{cases} \quad \text{where } \sigma_e > \sigma_p\,. \tag{2}$$

The noise variance of the programmed states is significantly smaller that the variance for the erased state because of a tight programming control loop using a small voltage step [14]. This is modeled by having $\sigma_e > \sigma_p$.

*2) Wear-out Noise:* Wear-out noise is caused by recurring P/E operations damaging the oxide layer through generation of oxide traps and interface traps. In [7], the authors point out that interface traps have the most significant impact on wear-out in deeply scaled devices; therefore, the impact of oxide traps is not considered in this component.

The wear-out effect of traps on measured thresholds can be modeled as Random Telegraph Noise (RTN). RTN widens the distribution of read thresholds with exponential tails on both sides of the actual threshold voltage [8]. However, based on the data from some real devices, the distribution of read thresholds can feature significant single-sided exponential tails in either the positive or negative direction. We use the following exponential distribution as the model for wear-out noise in this paper:

$$f_{N_W}(n_w) = \begin{cases} \frac{1}{\lambda} e^{-\frac{n_w}{\lambda}} & \text{if } n_w \geq 0 \\ 0 & \text{if } n_w < 0 \end{cases}, \tag{3}$$

where $\lambda$ is the channel parameter which functions as a metric for interface trap density.

*3) Retention Noise:* Retention loss is caused by electron detrapping. Thus, the characteristic of this noise component is determined by the interface trap density, oxide trap density and retention time [9]. Following [9], we model retention loss as Gaussian noise with distribution

$$f_{N_R}(n_r) = \frac{1}{\sigma_r\sqrt{2\pi}} e^{-\frac{(n_r-\mu_r)^2}{2\sigma_r^2}}, \qquad (4)$$

where

$$\mu_r = \gamma_{\mu_r}(x - x_0)\,, \qquad (5)$$

$$\sigma_r = \gamma_{\sigma_r}\sqrt{x - x_0}\,. \qquad (6)$$

The parameters $\gamma_{\mu_r}$ and $\gamma_{\sigma_r}$ represent trap density and retention time. Variable $x$ is the intended threshold, and $x_0$ is the intended erased-state threshold. Note that in this model, there is no retention loss if the intended threshold is that of the erased state.

*4) Overall Conditional Distribution for Flash Channel:* From the discussion above, the conditional distribution for Flash read channel can be summarized as

$$f_{Y|X}(y|x) = \frac{e^{\frac{\mu_r+x-y}{\lambda}+\frac{\sigma^2}{2\lambda^2}}}{\lambda} \cdot Q\left(\frac{\mu_r+x-y}{\sigma} + \frac{\sigma}{\lambda}\right), \qquad (7)$$

where $x$ is the intended threshold voltage and $y$ is the measured threshold voltage. The value of $\sigma$ depends on the intended voltage as follows:

$$\sigma = \begin{cases} \sqrt{\sigma_e^2 + \sigma_r^2} & \text{if } x = x_0 \\ \sqrt{\sigma_p^2 + \sigma_r^2} & \text{otherwise} \end{cases}. \qquad (8)$$

$Q(m)$ is the tail probability of the standard normal distribution: $Q(m) = \int_m^\infty \frac{e^{-x^2/2}}{\sqrt{2\pi}}\,dx$. The parameters $\sigma_r, \mu_r$ and $\lambda$ evolve over both time and P/E cycling process, as the channel degrades, while $\sigma_e$ and $\sigma_p$ remain constant. Given a specific retention time, P/E cycling condition, and the physics related parameters, the exact value of the current channel parameters can be determined using channel parameter degradation model proposed in [3].

## III. Binning Strategy for Histogram Measurement

A good binning strategy, i.e. selecting the proper number and placement of word line voltages for the reads that will create the histogram bins, is critical for the efficiency and accuracy of practical histogram-dependent signal processing methods in Flash.

### A. Number of Bins

A fairly accurate channel estimation can, of course, be derived from a complete voltage scan which uses the smallest possible bin width by reading at every available voltage level using the so-called debug mode. However, the large number of reads required by this process stalls normal operations. Such a large number of reads is likely not necessary. From the soft decoding literature [6], [15], [16], a relatively small number of read voltages is sufficient to give good performance in terms of both decoding and channel estimation.

Furthermore, too many bins in the histogram will cause high computational cost in each iteration of the least squares algorithms described in Section IV, and also require more storage space. Thus a relatively small number of bins can reduce both complexity and latency. The choice for the number of bins also depends on the channel estimation algorithm employed. Basic algorithms usually require more detailed channel measurements than advanced algorithms. As shown below in Sec. V, a 10-bin histogram can provide enough information for accurate estimations of the channel parameters in our model. Thus, in exploring the performance of the three bin-placement paradigms, we focus on the 10-bin case.

### B. Selecting a Bin-Placement Paradigm

We will consider three bin-placement paradigms: equal-width, equal-probability, and maximum mutual information (MMI). Equal-width histograms have bins covering intervals of equal length except for the semi-infinite bins at the leftmost and rightmost boundaries. Equal-probability histograms allocate bins having the same probability (i.e. the same number of occurrences in each bin). MMI word-line voltage placement proposed in [15], [16] optimizes decoding performance by maximizing the mutual information between the distribution of levels and the histogram bin identified when the cell is read.

As presented in Section IV, channel parameters are estimated by minimizing the squared Euclidean distance between the measured histogram acting as the reference and the histogram induced by the estimated channel parameters. To achieve good estimation accuracy, the measured histogram should be as close to the original channel distribution as possible. To compare bin-placement paradigms, the squared Euclidean distance between the channel distribution $f(y)$ and the histogram induced by $f(y)$ is used as the metric to evaluate the amount of discretization error of a bin-placement paradigm. This metric $D_{E^2}$ is defined as follows:

$$D_{E^2} = \sum_{i=0}^{M-1} \int_{q_i}^{q_{i+1}} \left( f(y) - \frac{H_i}{q_{i+1} - q_i} \right)^2 dy\,, \qquad (9)$$

where $f(y)$ is the true read channel distribution, $M$ is the number of bins, and $q_i, q_{i+1}$ represent the left and right boundary of the the $i$th interval. $H_i$ is the probability of $i$th bin induced by $f(y)$, $H_i = \int_{q_i}^{q_{i+1}} f(y)dy$, and $\frac{H_i}{q_{i+1}-q_i}$ denotes the probability density of the $i$th bin.

Fig. 3 shows $D_{E^2}$ with 10-bin histograms for the three bin-placement paradigms. The parameters provided in [3] are used to generate channel distributions as a function of the number of P/E cycles. The equal-probability bin placement provides a lower $D_{E^2}$, and hence a better approximation to the original channel, than the other two strategies over a large span of P/E cycling conditions. The performance difference is especially significant when the device condition is new. This behavior is also seen with 7 bins. As the number of bins grows, the performance difference becomes smaller, but a small number of bins is preferred in our application.

As a complement to $D_{E^2}$, effective resolution is a second metric with which to compare bin placement paradigms. Effective resolution represents the bin count of an ideal

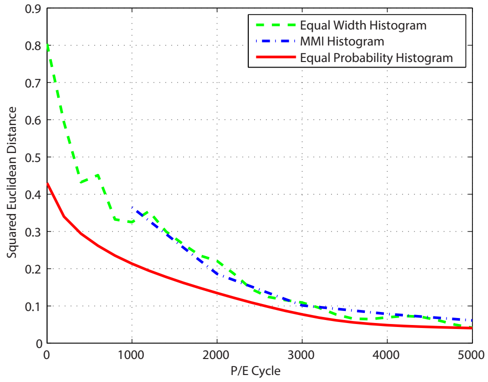


Fig. 3. Squared Euclidean distance between the channel distributions and corresponding histograms (10 bins).

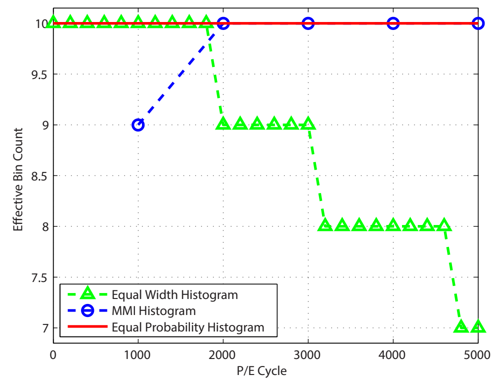


Fig. 4. Effective resolution of different histograms (10 bins).

non-redundant histogram that conveys the same amount of distribution shape information as the histogram under consideration. Because a read at the shared boundary of two zero-height bins does not provide additional information about the distribution, two adjacent zero-height bins can be combined as one. Effective resolution is essentially the bin count after combining adjacent zero-count bins.

Although histogram bin probabilities derived from integration of the channel model over the width of bins are nonzero, real measurements from a finite number of cells (e.g. a block) will often produce zero-count bins if the bin probability is efficiently small. Fig. 4 shows the effective resolution as a function of the number of P/E cycles for the three bin-placement paradigms. Adjacent bins with induced probability less than $10^{-4}$ are combined. The equal-probability bin-placement paradigm has full resolution throughout the entire P/E cycling process, while the other paradigms lose resolution in some P/E cycling conditions. This suggests that the equal-probability bin-placement paradigm has a good tracking capability over the whole Flash lifetime.

Because of the superior performance in terms of both $D_{E^2}$ and effective resolution, the equal-probability bin-placement paradigm is used in the channel parameter estimation discussed in the remainder of this paper.

## IV. Channel Parameter Estimation

### A. Cost Function

From the discussion in Section II, the channel parameter vector is $[\lambda, \sigma_p, \sigma_e, \sigma_r, \mu_r]$. However, both $\sigma_r$ and $\mu_r$ are dependent on the intended threshold voltage. Using (5) and (6) the voltage-independent channel parameter vector $\boldsymbol{\alpha} = [\lambda, \sigma_p, \sigma_e, \gamma_{\sigma_r}, \gamma_{\mu_r}]$ is used in the following discussion as the set of paramaters to be estimated. Voltage-independent channel parameters are preferred for supporting the DVA algorithm, which is a target application for HBCE.

Define $[q_0, q_1, \ldots, q_M]$ as the boundaries of the $M$ bins where $q_0 = -\infty$, and $q_M = \infty$. The expected number of cells in each bin can be computed as

$$\hat{N}_{bin,i} = \sum_{k=1}^{L} N_k P(q_i < y < q_{i+1} | x_k)\,, \tag{10}$$

where $P(q_i < y < q_{i+1}|x_k) = \int_{q_i}^{q_{i+1}} f_{Y|X}(y|x_k)\,dy$ denotes the probability of a measured threshold falling in the $i$th bin when the intended threshold is $x_k$ according to the channel probability distribution. $L$ is the number of intended threshold levels, and $N_k$ is the number of cells in each level for the stored data.

The cost function is defined as the normalized square Euclidean distance between the expected histogram induced by the estimated parameters and the reference histogram

$$C_M = \sum_{i=0}^{M-1} \left( \frac{N_{bin,i} - \hat{N}_{bin,i}}{N} \right)^2 , \tag{11}$$

where $N$ is the total number of cells measured, and $N_{bin,i}$ is the $i$th bin's cell count in the reference histogram. The gradient of the cost function is defined as

$$\nabla \boldsymbol{C}_M(\boldsymbol{\alpha}) = 2 \cdot (\boldsymbol{J}_{\boldsymbol{G}_M}(\boldsymbol{\alpha}))^T \cdot \boldsymbol{G}_M(\boldsymbol{\alpha})\,, \tag{12}$$

where $\boldsymbol{J}_{\boldsymbol{G}_M}(\boldsymbol{\alpha})$ is the Jacobian matrix of the normalized difference vector $\boldsymbol{G}_M$ between the estimated histogram and the measured histogram.

### B. Least Squares Algorithms

Least squares algorithms have been widely used to fit a parameterized model to a data set. Three algorithms are examined in the following discussion.

*1) Gradient Descent (GD):* GD minimizes the cost function by refining initial estimation of the parameters based on a linear approximation. In each iteration, the estimation is renewed by a step vector following the gradient of the cost function.

**Algorithm 1** Gradient Descent Algorithm

Initialize step size $\beta$ and $\boldsymbol{\alpha} = \boldsymbol{\alpha}^{(0)}$
**while** $\|\boldsymbol{\alpha}^{(k+1)} - \boldsymbol{\alpha}^{(k)}\| > \eta$ and $k < MaxIteration$ **do**
    Compute $\boldsymbol{J}_{\boldsymbol{G}_M}(\boldsymbol{\alpha}^{(k)})$ and $\boldsymbol{G}_M(\boldsymbol{\alpha}^{(k)})$
    Compute $\nabla C_M(\boldsymbol{\alpha}^{(k)}) = 2 \cdot (\boldsymbol{J}_{\boldsymbol{G}_M}(\boldsymbol{\alpha}^{(k)})^T \cdot \boldsymbol{G}_M(\boldsymbol{\alpha}^{(k)})$
    $\boldsymbol{\alpha}^{(k+1)} = \boldsymbol{\alpha}^{(k)} - \beta \cdot \nabla \boldsymbol{C}_M(\boldsymbol{\alpha}^{(k)})$
    $k = k + 1$
**end while**

*2) Gauss-Newton (GN):* A quadratic model is employed to provide more accurate approximations of the cost function. The iterative relation can be represented as

$$\boldsymbol{\alpha}^{(k+1)} = \boldsymbol{\alpha}^{(k)} - (\boldsymbol{J}^T\boldsymbol{J})^{-1}\boldsymbol{J}^T\boldsymbol{G} = \boldsymbol{J}^{+}\boldsymbol{G}\,, \tag{13}$$

where $\boldsymbol{J}^+$ is the pseudo-inverse of $\boldsymbol{J}$. Gauss-Newton algorithm can then be formulated as follows:

**Algorithm 2** Gauss-Newton Algorithm

Initialize $\boldsymbol{\alpha} = \boldsymbol{\alpha}^{(0)}$
**while** $\|\boldsymbol{\alpha}^{(k+1)} - \boldsymbol{\alpha}^{(k)}\| > \eta$ and $k < MaxIteration$ **do**
    Compute $\boldsymbol{J}_{\boldsymbol{G}_M}(\boldsymbol{\alpha}^{(k)})$ and $\boldsymbol{G}_M(\boldsymbol{\alpha}^{(k)})$
    $\boldsymbol{\alpha}^{(k+1)} = \boldsymbol{\alpha}^{(k)} - (\boldsymbol{J}_{\boldsymbol{G}_M}(\boldsymbol{\alpha}^{(k)}))^{+} \cdot \boldsymbol{G}_M(\boldsymbol{\alpha}^{(k)})$
    $k = k + 1$
**end while**

*3) Levenberg-Marquardt (LM) [17]:* By combining GD and GN, LM possesses the advantages of both algorithms. The update vector $\boldsymbol{\delta}_{\boldsymbol{\alpha}}$ is calculated by solving $(\boldsymbol{J}^T\boldsymbol{J} + \beta \cdot \mathrm{diag}((\boldsymbol{J}_{\boldsymbol{G}_M})^T\boldsymbol{J}_{\boldsymbol{G}_M}))\boldsymbol{\delta}_{\boldsymbol{\alpha}} = \boldsymbol{J}^T\boldsymbol{G}$ where $\beta$ acts as a weight to combine the two algorithms.

**Algorithm 3** Levenberg-Marquardt Algorithm

Initialize $\beta, v, \boldsymbol{\alpha} = \boldsymbol{\alpha}^{(0)}$ and $UpdateFlag = 1$
**while** $\|\boldsymbol{\alpha}^{(k+1)} - \boldsymbol{\alpha}^{(k)}\| > \eta$ and $k < MaxIteration$ **do**
    **if** $UpdateFlag = 1$ **then**
        Compute $\boldsymbol{J}_{\boldsymbol{G}_M}(\boldsymbol{\alpha}^{(k)})$ and $\boldsymbol{G}_M(\boldsymbol{\alpha}^{(k)})$
    **end if**
    Solve $((\boldsymbol{J}_{\boldsymbol{G}_M})^T\boldsymbol{J}_{\boldsymbol{G}_M} + \beta \cdot diag((\boldsymbol{J}_{\boldsymbol{G}_M})^T\boldsymbol{J}_{\boldsymbol{G}_M}))\boldsymbol{\delta}_{\boldsymbol{\alpha}} = (\boldsymbol{J}_{\boldsymbol{G}_M})^T\boldsymbol{G}_M$
    Compute $\boldsymbol{J}_{\boldsymbol{G}_M}(\boldsymbol{\alpha}^{(k)})$ and $\boldsymbol{G}_M(\boldsymbol{\alpha}^{(k)})$
    $\boldsymbol{\alpha}_{temporary} = \boldsymbol{\alpha} - \boldsymbol{\delta}_{\boldsymbol{\alpha}}$
    **if** $\sum(err(\boldsymbol{\alpha}))^2 > \sum(err(\boldsymbol{\alpha}_{temporary}))^2$ **then**
        $UpdateFlag = 1$
        $\beta = \beta \cdot v$
        $\boldsymbol{\alpha} = \boldsymbol{\alpha}_{temporary}$
    **else**
        $UpdateFlag = 0$
        $\beta = \beta / v$
    **end if**
    $k = k + 1$
**end while**

## V. Simulation Results

To verify the effectiveness of the algorithms described in Section IV and determine the number of reads needed for equal-probability bin-placement paradigm, channel distributions generated with parameters from [3] are used in our simulations. The retention time is set to be one year. P/E cycling conditions from 0 to 4000 P/E are sampled every 300 P/E creating fourteen channels. The initial conditions for the three algorithms are the same [0.007,0.1,0.4,0.04,-0.4]. For the channel corresponding to 3000 P/E cycles, Fig. 5 compares the actual channel PDF with the PDF induced by the estimated channel parameters.

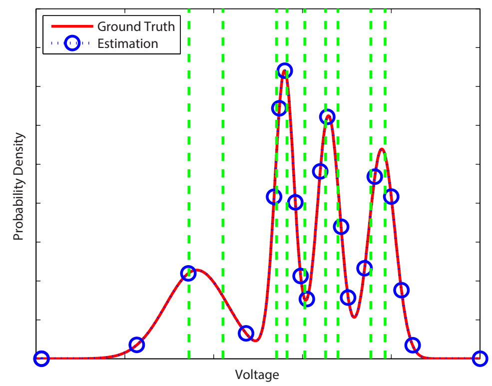


Fig. 5. Channel estimation result at 3000 P/E cycles using Levenberg-Marquardt algorithm and 10-bin equal-probability histogram. (ground truth parameter vector is [0.0099,0.3500,0.0500,0.0617,-0.5882], estimation error vector is $10^{-4}\times$[0.0101 0.0214 -0.1774 0.0405 -0.0044])

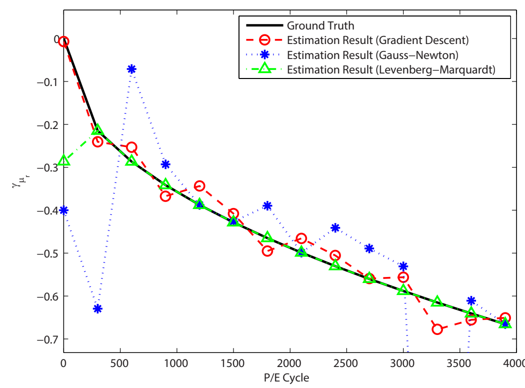


Fig. 6. Estimation result versus ground truth for $\gamma_{\mu_r}$ using 10-bin equal-probability histogram.

Fig. 6 compares the estimating results of $\gamma_{\mu_r}$ with the ground truth, where the estimation algorithms employ 10-bin equal-probability histograms as input. The LM algorithm performs significantly better than GD and GN in terms of both the estimation accuracy and the ability to adapt to different channel conditions.

This behavior is further demonstrated in Table I, which shows the convergence counts of the three algorithms over the 14 channels. Every estimated parameter needs to be within $\pm 1\%$ of the ground truth parameter to qualify as a converged result. GD fails in all simulation cases while reaching the maximum allowed number of iterations in every case. GN provides good results in certain cases with very few iterations. LM provides high estimation accuracy over different channel conditions, with some failures when the channel conditions are very good. Note that estimation accuracy of $\gamma_{\sigma_r}$ is usually

TABLE I
Converge counts of least square algorithms (over 14 cases).

| No. of Reads | GD | GN | LM |
|---|---|---|---|
| 6 | 0 | 1 | 12 |
| 9 | 0 | 3 | 13 |
| 12 | 0 | 4 | 11 |

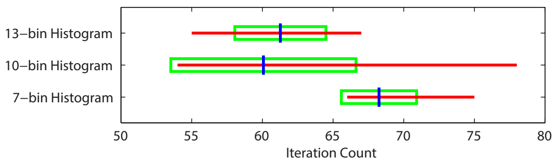


Horizontal Line Segment: Range of Iteration Count
Vertical Line Segment: Mean of Iteration Count
Rectangle: Standard Deviation of Iteration Count

Fig. 7. Iteration count statistics using Levenberg-Marquardt algorithm.

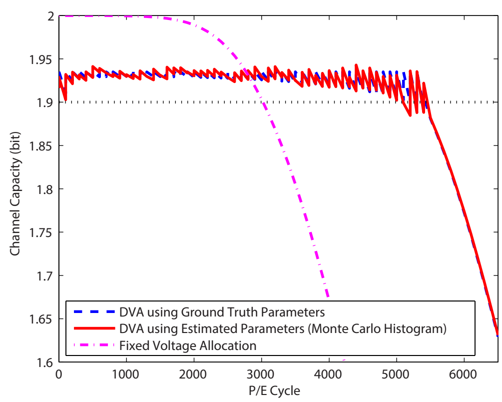


Fig. 8. Dynamic Voltage Allocation simulation result.

higher than the other parameters. An intuitive explanation for this is that channel distribution mean shifts can be easily identified by even the histogram itself.

Fig. 7 depicts key statistical metrics about the number of iterations when employing LM with histograms that differ in resolution over the 14 cases. 10-bin (9-read) histograms reduce the number of iterations needed with respect to the results using 7-bin (6-read) histograms. 13-bin (12-read) histograms do not provide significant reduction in iteration counts. We conjecture that the 10-bin histogram provides good performance as it strikes the right balance. If the number of bins is too small, then too many channels can match the measured histogram so that the optimization cannot get a clear direction. If the number of bins is too large, the estimation problem is over-constrained, which slows convergence. The computational complexity of each iteration is related to both the histogram and the channel model. With the complexity of our model and the need for adaptively updating the bin placement, we expect the overall complexity of the estimation framework to be higher than [6].

We have successfully used the LM algorithm with a 10-bin histogram for a DVA [3] algorithm. As shown in Fig. 8, the performance using histogram generated by Monte Carlo histogram is not distinguishable from the performance with perfect knowledge of the channel.

## VI. Conclusion

This paper introduces a framework to estimate dynamically changing Flash memory channels by applying least squares algorithms to measured histograms. Our analysis and simulation results show that good estimation accuracy and speed can be achieved by using Levenberg-Marquardt algorithm with 10-bin equal-probability histograms. With this framework, Flash channel estimation can support performance enhancing techniques such as Dynamic Voltage Allocation.

## References

[1] Y. Maeda and H. Kaneko, "Error control coding for multilevel cell flash memories using nonbinary low-density parity-check codes," in *Defect and Fault Tolerance in VLSI Systems, 2009. DFT '09. 24th IEEE International Symposium on*, Oct. 2009, pp. 367–375.

[2] T. Klove, B. Bose, and N. Elarief, "Systematic, single limited magnitude error correcting codes for flash memories," *Information Theory, IEEE Transactions on*, vol. 57, no. 7, pp. 4477–4487, Jul. 2011.

[3] T.-Y. Chen, A. R. Williamson, and R. D. Wesel, "Increasing flash memory lifetime by dynamic voltage allocation for constant mutual information," in *Information Theory and Applications Workshop (ITA), 2014*, Feb. 2014, pp. 1–5.

[4] F. Sala, R. Gabrys, and L. Dolecek, "Dynamic threshold schemes for multi-level non-volatile memories," *Communications, IEEE Transactions on*, vol. 61, no. 7, pp. 2624–2634, Jul. 2013.

[5] R. Bez, E. Camerlenghi, A. Modelli, and A. Visconti, "Introduction to flash memory," *Proceedings of the IEEE*, vol. 91, no. 4, pp. 489–502, Apr. 2003.

[6] D.-h. Lee and W. Sung, "Estimation of NAND flash memory threshold voltage distribution for optimum soft-decision error correction," *Signal Processing, IEEE Transactions on*, vol. 61, no. 2, pp. 440–449, Jan. 2013.

[7] J.-D. Lee, J.-H. Choi, D. Park, and K. Kim, "Data retention characteristics of sub-100 nm NAND flash memory cells," *Electron Device Letters, IEEE*, vol. 24, no. 12, pp. 748–750, Dec. 2003.

[8] C. Monzio Compagnoni, M. Ghidotti, A. Lacaita, A. Spinelli, and A. Visconti, "Random telegraph noise effect on the programmed threshold-voltage distribution of flash memories," *Electron Device Letters, IEEE*, vol. 30, no. 9, pp. 984–986, Sep. 2009.

[9] N. Mielke, H. Belgal, A. Fazio, Q. Meng, and N. Righos, "Recovery effects in the distributed cycling of flash memories," in *Reliability Physics Symposium Proceedings, 2006. 44th Annual., IEEE International*, Mar. 2006, pp. 29–35.

[10] R.-A. Cernea, L. Pham, F. Moogat, S. Chan, B. Le, Y. Li, S. Tsao, T.-Y. Tseng, K. Nguyen, J. Li, J. Hu, J. H. Yuh, C. Hsu, F. Zhang, T. Kamei, H. Nasu, P. Kliza, K. Htoo, J. Lutze, Y. Dong, M. Higashitani, J. Yang, H.-S. Lin, V. Sakhamuri, A. Li, F. Pan, S. Yadala, S. Taigor, K. Pradhan, J. Lan, J. Chan, T. Abe, Y. Fukuda, H. Mukai, K. Kawakami, C. Liang, T. Ip, S.-F. Chang, J. Lakshmipathi, S. Huynh, D. Pantelakis, M. Mofidi, and K. Quader, "A 34 MB/s MLC write throughput 16 gb NAND with all bit line architecture on 56 nm technology," *Solid-State Circuits, IEEE Journal of*, vol. 44, no. 1, pp. 186–194, Jan. 2009.

[11] Y. Cai, O. Mutlu, E. Haratsch, and K. Mai, "Program interference in MLC NAND flash memory: Characterization, modeling, and mitigation," in *Computer Design (ICCD), 2013 IEEE 31st International Conference on*, Oct. 2013, pp. 123–130.

[12] G. Dong, Y. Pan, and T. Zhang, "Using lifetime-aware progressive programming to improve SLC NAND flash memory write endurance," *Very Large Scale Integration (VLSI) Systems, IEEE Transactions on*, vol. PP, no. 99, pp. 1–1, 2013.

[13] K. Takeuchi, T. Tanaka, and H. Nakamura, "A double-level-vth select gate array architecture for multilevel NAND flash memories," *Solid-State Circuits, IEEE Journal of*, vol. 31, no. 4, pp. 602–609, Apr. 1996.

[14] C. Compagnoni, A. Spinelli, R. Gusmeroli, A. Lacaita, S. Beltrami, A. Ghetti, and A. Visconti, "First evidence for injection statistics accuracy limitations in NAND flash constant-current fowler-nordheim programming," in *Electron Devices Meeting, 2007. IEDM 2007. IEEE International*, Dec. 2007, pp. 165–168.

[15] J. Wang, T. Courtade, H. Shankar, and R. Wesel, "Soft information for LDPC decoding in flash: Mutual-information optimized quantization," in *Global Telecommunications Conference (GLOBECOM 2011), 2011 IEEE*, Dec. 2011, pp. 1–6.

[16] J. Wang, K. Vakilinia, T.-Y. Chen, T. Courtade, G. Dong, T. Zhang, H. Shankar, and R. Wesel, "Enhanced precision through multiple reads for LDPC decoding in flash memories," *Selected Areas in Communications, IEEE Journal on*, vol. 32, no. 5, pp. 880–891, May 2014.

[17] D. W. Marquardt, "An algorithm for least-squares estimation of nonlinear parameters," *Journal of the Society for Industrial and Applied Mathematics*, vol. 11, no. 2, pp. pp. 431–441, 1963. [Online]. Available: http://www.jstor.org/stable/2098941